GEOPHYSICS, VOL. 68, NO. 4 (JULY-AUGUST 2003); P. 1380–1388, 9 FIGS.
10.1190/1.1598131

# Traveltime calculations from frequency-domain downward-continuation algorithms

Changsoo Shin*, Seungwon Ko*, Wonsik Kim*, Dong-Joo Min‡, Dongwoo Yang*, Kurt J. Marfurt**, Sungryul Shin§, Kwangjin Yoon*, and Cheol Ho Yoon§§

**ABSTRACT**

We present a new, fast 3D traveltime calculation algorithm that employs existing frequency-domain wave-equation downward-continuation software. By modifying such software to solve for a few complex (rather than real) frequencies, we are able to calculate not only the first arrival and the approximately most energetic traveltimes at each depth point but also their corresponding amplitudes. We compute traveltimes by either taking the logarithm of displacements obtained by the one-way wave equation at a frequency or calculating derivatives of displacements numerically. Amplitudes are estimated from absolute value of the displacement at a frequency.

By using the one-way downgoing wave equation, we also circumvent generating traveltimes corresponding to near-surface upcoming head waves not often needed in migration. We compare the traveltimes computed by our algorithm with those obtained by picking the most energetic arrivals from finite-difference solutions of the one-way wave equation, and show that our traveltime calculation method yields traveltimes comparable to solutions of the one-way wave equation. We illustrate the accuracy of our traveltime algorithm by migrating the 2D IFP Marmousi and the 3D SEG/EAGE salt models.

## INTRODUCTION

Correct and efficient traveltime calculation is of critical importance for transmission tomography, refraction tomography, earthquake seismology, and prestack Kirchhoff migration. Geophysicists have developed a variety of traveltime calculation techniques from simple shooting ray-tracing techniques through two-point ray-tracing methods to finite-difference approximations of the eikonal equation.

The ray-shooting and two-point ray-tracing methods (Cerveny et al., 1977; Cassell, 1982; Um and Thurber, 1987) were the methods of choice to calculate traveltimes until the finite-difference solution of the eikonal equation provided a faster alternative. Although the ray-based techniques produce accurate traveltimes, they suffer from shadow zones and require subsequent interpolation onto a rectilinear grid. The finite difference solution of the eikonal equation (Vidale, 1988) avoids these problems by computing first-arrival traveltimes using expanding square cells. For models with percentage velocity contrasts greater than $\sqrt{2}$, however, Vidale's original method fails to correctly compute global minimum traveltimes. For accurate first-arrival calculation methods, Vidale's method was modified by Qin et al. (1990), Podvin and Lecomte (1991), Popovici (1991a, b), van Trier and Symes (1991), Cao and Greenhalgh (1994), and Schneider (1995). Coultrip (1993) devised a somewhat different wavefront-tracing method which finds a global minimum time path using triangular rather than rectangular cells. Sethian and Popovici (1999) also developed a fast marching method for solving the eikonal equation, which constructs entropy-satisfying approximations to the gradient term of the arrival time. All of these methods calculate the first-arrival traveltimes.

Although first-arrival traveltimes are commonly used in Kirchhoff migration, Geoltrain and Brac (1993) and Nichols

Published on Geophysics Online March 10, 2003. Manuscript received by the Editor May 12, 2000; revised manuscript received February 7, 2003.
*Seoul National University, School of Civil, Urban and Geosystem Engineering San 56-1, Shillim-Dong, Kwanak-ku, Seoul, 151-742, Korea. E-mail: css@model.snu.ac.kr; gplko@msn.com; wskim@gpl.snu.ac.kr; dwyang@gpl.snu.ac.kr; kjyoon@gpl.snu.ac.kr.
‡Korea Ocean Research and Development Institute, Marine Environment and Climate Change Laboratory, Ansan P.O. Box 29, Kyungki, 425-600, Korea. E-mail: djmin@kordi.re.kr.
**University of Houston, Allied Geophysical Laboratories, Department of Geoscience, Houston, Texas 77204-5006. E-mail: kmarfurt@uh.edu.
§Korea Maritime University, Department of Energy and Resources Engineering, #1 Dongsam-Dong, Youngdo-Gu, Pusan, 606-791, Korea. E-mail: srshin@hahara.kmaritime.ac.kr.
§§Sunmoon University, Department of Industrial Engineering, Galsanri Tangjeong-myum, Asan, Chungnam, 336-708, Korea. E-mail: yoonch@sunmoon.ac.kr.

(1996) asserted that, for complex structures such as the Marmousi model, Kirchhoff migration using first-arrival traveltimes can yield inferior images, because the first-arrival traveltimes often represent small-energy events rather than later events containing more significant energy. To address this problem, Nichols (1996) solved the paraxial one-way wave equation in polar coordinates for 8–16 frequencies, from which he was able to estimate the traveltime, amplitude, and phase of the most energetic arrival event. Nichols (1996) showed that the Kirchhoff migration image obtained by using the most energetic traveltime method is comparable to that produced by the much more expensive wave equation methods. Multipath, multitraveltime Kirchhoff migration (Sun, 1992; Vinje et al., 1999) produces further improvement yet, but keeping track of such traveltimes becomes cumbersome in three-dimensions.

In this paper, we present a new traveltime calculation method which gives traveltimes comparable to those predicted by the one-way wave equation. Our method calculates the traveltimes and amplitudes of either the first-arrival event or the approximately most energetic arrivals from one- or three-frequency solutions obtained by any of the commonly used one-way wave equation techniques: paraxial, split step, phase shift and interpolation, and phase shift with finite differences. We favor the paraxial equation and have implemented a particularly efficient 3D implicit one-way wave-equation solver based on nested dissection matrix factorization technology (George and Liu, 1981). For typical earth geologies, the use of a one-way downgoing wave equation helps us to eliminate traveltimes corresponding to upcoming head waves and multiples which are not often needed in migration.

Our eventual goal is to reduce the number of frequencies needed in obtaining traveltimes which will be used in our migration algorithm. We begin by reviewing the wave propagation properties of Claerbout's (1985) one-way wave equation. We then explain a simple technique that computes traveltime and amplitude that we can use in Kirchhoff migration. Next, we demonstrate the accuracy of our method by comparing the traveltimes computed by our method with those obtained by using the one-way wave equation for the 2D Marmousi model. Finally, we generate Kirchhoff-migrated images by using the traveltimes computed with our algorithm for the 2D Marmousi and the 3D SEG/EAGE salt models.

## THEORY

### One-way wave equation

For concreteness of discussion, we illustrate our traveltime calculation using Claerbout's (1985) one-way wave equation. We write a modified 87° one-way wave equation (Berkhout, 1979; Ma, 1981; Lee and Suh, 1985) in the frequency domain as

$$\frac{\partial U(x,y,z,\omega)}{\partial z} = i\frac{\omega}{v(x,y,z)} \times \left[1 + \sum_{k=1}^{n} \frac{\alpha_k(\partial_{xx}+\partial_{yy})}{\left(\frac{\omega}{v(x,y,z)}\right)^2 + \beta_k(\partial_{xx}+\partial_{yy})}\right] \times U(x,y,z,\omega) + f(x,y,z), \quad (1)$$

where $n$ is the order of the Padé approximation to the one-way wave equation, $\alpha_k$ and $\beta_k$ are the coefficients that minimize the dispersion (Lee and Suh, 1985), $U(x,y,z,\omega)$ is the wavefield, $x$ and $y$ are the horizontal coordinates, $z$ is the vertical coordinate, $\omega$ is the angular frequency, $\partial_{xx}$ and $\partial_{yy}$ are the operators representing the second-order partial derivative operator with respect to $x$ and $y$, respectively, $f(x,y,z)$ is the source function, and $v(x,y,z)$ is the velocity. If we wished to obtain the impulse response of this one-way wave equation, we would solve equation (1) using finite differences for a suite of frequencies and then synthesize the results by

$$u(x,y,z,t) = \int_{-\omega\max}^{\omega\max} U(x,y,z,\omega)e^{i\omega t}d\omega. \quad (2)$$

Unlike the classical hyperbolic wave equation, the wavefield $u$ in the one-way wave equation only propagates downward and therefore does not produce any vertically traveling multiples and upgoing head waves.

### Two new traveltime-and-amplitude calculation methods

We calculate traveltime and amplitude from the wavefield obtained by inserting a complex angular frequency into the one-way wave equation. In forward modeling, a complex angular frequency

$$\omega_\epsilon = \omega + i\epsilon, \quad (3)$$

where $\omega$ is the real angular frequency and $\epsilon$ is the wrap-around suppression factor, is commonly used to prevent wrap-around effects inherent in frequency-domain solutions. By virtue of the shifting theorem of Fourier transforms (see Appendix A), the factor $\epsilon$ suppresses the time-domain solutions by $e^{-\epsilon t}$. In conventional frequency-domain modeling, we synthesize our time-domain solutions from the Fourier components $\omega_\epsilon$, where $\epsilon$ is a constant and $\omega$ varies, and multiply the final time-domain results by the inverse of the damping factor, $e^{+\epsilon t}$.

In one-way wave equation modeling, this wrap-around suppression factor both stabilizes and suppresses wrap around in the solution (e.g., Figure 1). In Figure 1, the snapshot obtained with real frequencies (which is practically computed by $\epsilon = 1$) shows multiple events, whereas that with complex angular frequencies ($\epsilon = 80$) displays a single event. By using complex angular frequencies, we can reduce the general multiple event response to a single event. The resulting single event can correspond to either the first arrival or the most energetic event, depending on the frequency and the velocity model.

By trial and error, we found an empirical relationship between the wrap-around suppression factor and the grid size:

$$\epsilon \approx \frac{2\pi V_{\text{ave}}}{15 \times \Delta}, \quad (4)$$

where $\Delta$ is the maximum grid size and $V_{\text{ave}}$ is the average velocity in a model. If the grid size is determined to minimize numerical dispersion as is in a full wave equation (e.g., Shin et al., 2002), the optimal suppression factor $\epsilon$ is determined by equation (4).

We assume that the time-domain wavefield obtained by using the one-way wave equation with complex angular frequency can be approximated as

$$u(x,y,z,t) = \tilde{A}(x,y,z)\delta(t - \tau(x,y,z)), \quad (5)$$

where

$$\tilde{A}(x, y, z) = A(x, y, z)e^{-\epsilon t}, \tag{6}$$

and where $u$ is the wavefield, $\tau(x, y, z)$ is the traveltime from the source to a depth point in the subsurface, $A(x, y, z)$ is the amplitude at the depth point in the subsurface, and $\delta$ is the Dirac delta function. Equation (5) can be written in the frequency domain as

$$U(x, y, z, \omega) = \tilde{A}(x, y, z)e^{-i\omega\tau(x,y,z)}. \tag{7}$$

We can calculate traveltimes by two methods: one is to take the logarithm of both sides of equation (7); the other is to calculate derivative of displacement $U(x, y, z, \omega)$ with respect to angular frequency $\omega$. The first method is expressed by

$$\ln U(x, y, z, \omega) = \ln|\tilde{A}(x, y, z)| - i\omega\tau(x, y, z). \tag{8}$$

If we divide the imaginary component of equation (8) by the real angular frequency $\omega$, we can obtain the traveltime at each depth point. Although the angular frequency can, in principle, be selected arbitrarily, we propose to choose a low frequency to avoid cycle skipping effect inherent in calculating phase spectra (traveltimes). When we use a higher frequency, we need to convert the wrapped phase into an unwrapped phase, in which case we need to know the phase values for several frequencies (e.g., Osman and Robinson, 1996). Applying the phase-unwrapping algorithm to our method would be troublesome. For this reason, we propose a second method that does not suffer from cycle skipping effect and better approximates the most energetic traveltimes within the seismic frequency band.

Differentiating equation (7) with respect to $\omega$ gives

$$\frac{dU(x, y, z, \omega)}{d\omega} \approx -i\tau(x, y, z)\tilde{A}(x, y, z)e^{-i\omega\tau(x,y,z)} = -i\tau(x, y, z)U(x, y, z, \omega). \tag{9}$$

From equation (9), we compute the traveltime by dividing $(dU/d\omega)$ by $iU$. The derivative of $U$ with respect to $\omega$ can be calculated using either forward, backward, or central finite-difference approximations at two adjacent frequencies.

The only disadvantage of the second method is that we may lose accuracy at those depth points where the amplitudes of events following the first-arrival events are similar to or greater than that of the first-arrival event. However, we will show that the second method partly gives a very close approximation to the most energetic traveltimes at most depth points. The pathological case where the amplitude of damped later arrival event is greater than or equal to that of the first-arrival event requires further study.

In order to obtain improved migrated images, we need not only the most energetic traveltime but also the corresponding amplitude. Suppose that the one-way wave equation seismogram consists of fewer events than the original hyperbolic equation seismogram and that the most energetic amplitude is large enough, compared with other events, the most energetic arrival amplitude is dominant in the wavefield calculated by one-way wave equation at seismic frequency band. We

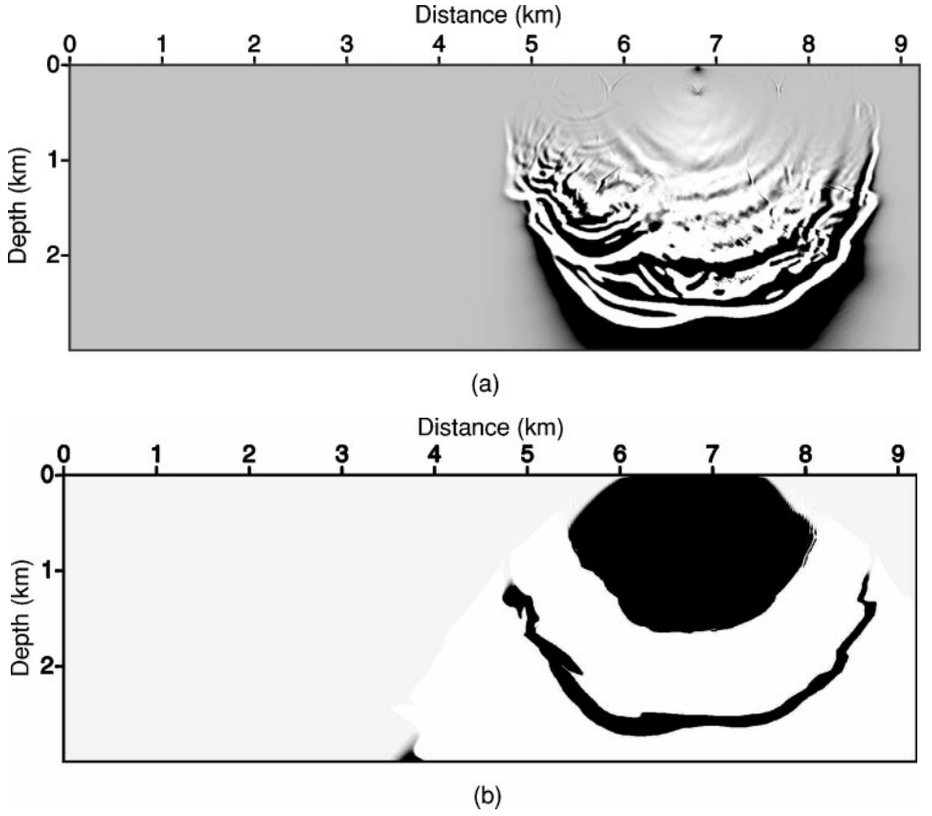


FIG. 1. Snapshot obtained from the one-way wave equation using (a) real frequencies (which are practically approximated by $\epsilon = 1$) and (b) complex angular frequencies ($\epsilon = 80$).

qualitatively express the approximately most energetic amplitude as an absolute value of the frequency-domain wavefield ($|A| \approx |U(x, y, z, \omega)|$) with a frequency; that is,

$$|\tilde{A}| = |A|e^{-\epsilon t} = |U|, \tag{10}$$

$$|A| = |U|e^{\epsilon t}. \tag{11}$$

We note that the amplitude computed by equation (11) does not have polarity change, because we take the absolute value. When we compute amplitude, we use a much smaller damping factor $\epsilon$ than that applied to obtain traveltime. The main reason for choosing the small damping factor is to avoid the computer precision limits of our 32-bit computer.

## NUMERICAL EXAMPLES

In order to evaluate how accurately our two algorithms calculate traveltimes, we first examine a homogeneous half-space model with a constant velocity of 1500 m/s. We describe the model using a $401 \times 201$ grid with a grid interval of 5 m in both $x$ and $z$ directions. We locate a source at the center of the surface. Since the two methods (taking logarithm of the displacement and using derivative of displacement with respect to $\omega$) give the same results for the homogeneous model, we simply display traveltimes calculated using the second method in Figure 2a. We display the absolute errors between the computed and the analytic traveltimes in Figure 2b. In Figure 2b, all of the errors are less than 0.0055 s with the average error being 0.0025 s.

We next compare the traveltimes obtained by our two methods with the most energetic traveltimes produced by finite-difference modeling solutions of the one-way wave equation.

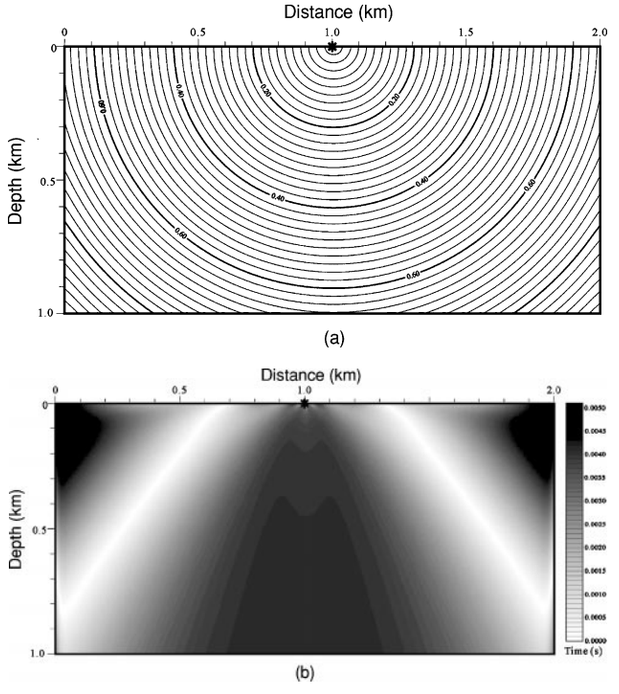


FIG. 2. (a) Traveltime contours of the homogeneous half-space model whose velocity is 1500 m/s. (b) Absolute errors between the analytic traveltimes and those calculated by our algorithm.

In Figure 3, we display the traveltime contours computed by the first algorithm (taking logarithm of the displacement) and the second algorithm (using the derivative of displacement with respect to $\omega$) as well as the most energetic traveltime contours for the 6%-smoothed Marmousi model. The degree of smoothing is measured by

$$\text{Degree of smoothing} = \sum_i \frac{|v_{i,h} - v_{i,s}|}{v_{i,h}} \times 100, \tag{12}$$

where $v_{i,h}$ and $v_{i,s}$ are the velocity at the $i$th grid of the hard and smoothed Marmousi models. From Figure 3, we note that the traveltimes computed by the first and the second algorithm show good agreement with the most energetic traveltimes at early times from 0.0 to 0.9 s. For later times, traveltimes obtained by the second method more closely approach the most energetic traveltimes than those of the first method (denoted by arrow). At the contour of 1.1 s, we also see the erroneous traveltimes obtained by the second method, which is associated with shadow zone (e.g., Figure 4a) of the Marmousi model. We also compute the absolute values of amplitudes using equation (11) and compare them with the absolute values of the most energetic amplitudes obtained from one-way wave equation solutions (see Figure 4). From Figure 4, we know that our amplitudes are compatible with the most energetic amplitudes. Next, we check whether or not the traveltimes obtained by our algorithms yield good migration images. Figure 5 shows prestack Kirchhoff migration images generated for the smoothed Marmousi structure using the most energetic traveltimes (picked from all-frequency finite-difference solutions) and those calculated at one or two frequencies by our two algorithms. In Figure 5, we note that the most energetic traveltimes picked from finite-difference solutions give the best image, whereas the traveltimes obtained by the second method (differentiating displacements with respect to $\omega$) produce a better image and a better resolved reservoir (arrow) than the first method (taking logarithm of single-frequency displacements). We add the approximately most energetic amplitudes to the

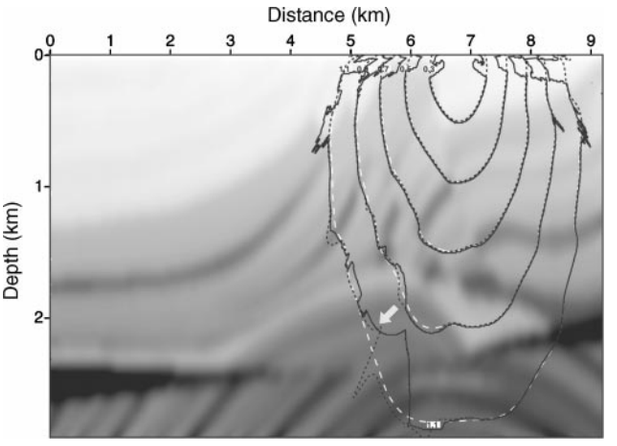


FIG. 3. The most energetic traveltime contours (black solid line) obtained from picking snapshot generated by the finite-difference solutions of the one-way wave equation, and traveltime contours by the first (white dashed line) and the second method (black dotted line) for the 6%-smoothed Marmousi model.

corresponding traveltimes to our standard Kirchhoff migration and display the image shown in Figure 6. Even though we do not account for polarity change in the amplitudes, we obtain better resolved fault planes and reservoir (arrows) than when only using traveltime (e.g., Figures 5c and 6).

To proceed further, we computed traveltimes using two algorithms for the 3D SEG/EAGE salt model. The velocity model selected for comparing the traveltimes is located from 5 km to 8.98 km along the $x$ direction, from 2 km to 5.98 km along the $y$ direction, and from 0 to 1.4 km along the $z$ direction. The grid spacing is 20 m in the $x$, $y$, and $z$ directions. A source is located at the (6.99 km, 3.99 km, 0 km) point. In Figure 7, we overlay traveltime contours computed by our two algorithms on the salt velocity model. Figures 7a and 7b show the traveltime contours of the inline section at $x = 6.99$ km and crossline section at $y = 3.99$ km, whereas Figure 7c shows the traveltime contours at the depth $z = 1.4$ km. From Figures 7a, 7b, and 7c, we could speculate that the distorted contours of the traveltimes that were generated by the second algorithm (denoted by arrows) result from multiple events with nearly the same amplitudes as or larger amplitudes than that of the first-arrival event.

Having finished the traveltime computation for the 3D SEG/EAGE salt model, we proceeded to migrate the salt model data. Figures 8 and 9 show the prestack Kirchhoff migration images generated for the salt model using the traveltimes calculated by the first and second traveltime calculation algorithms. Figures 8a and 9a show the images of the inline at $x = 8.84$ km, whereas Figures8b and 9b show the images of the crossline at $y = 5.74$ km. Figures 8c and 9c show the images at $z = 0.64$ km. From Figures 8 and 9, we note that the second traveltime calculation algorithm using partial derivatives of the displacements provides better images at the horizontal layers below 3.5 km in depth than the first algorithm using the logarithm of the displacements. The total cost of Kirchhoff migration including the cost of the traveltime calculation for the 3D SEG/EAGE narrow-azimuth salt data using an aperture of 3 km × 1 km was 100 hours on 12 IBM Regatta power 4 processors running under MPI.

## COMPUTATIONAL EFFICIENCY

Zhu and Lines (1998) showed that for 2D Kirchhoff migration, traveltime computation takes 40% of total computational effort, and Kirchhoff migration takes 60%. In 3D Kirchhoff

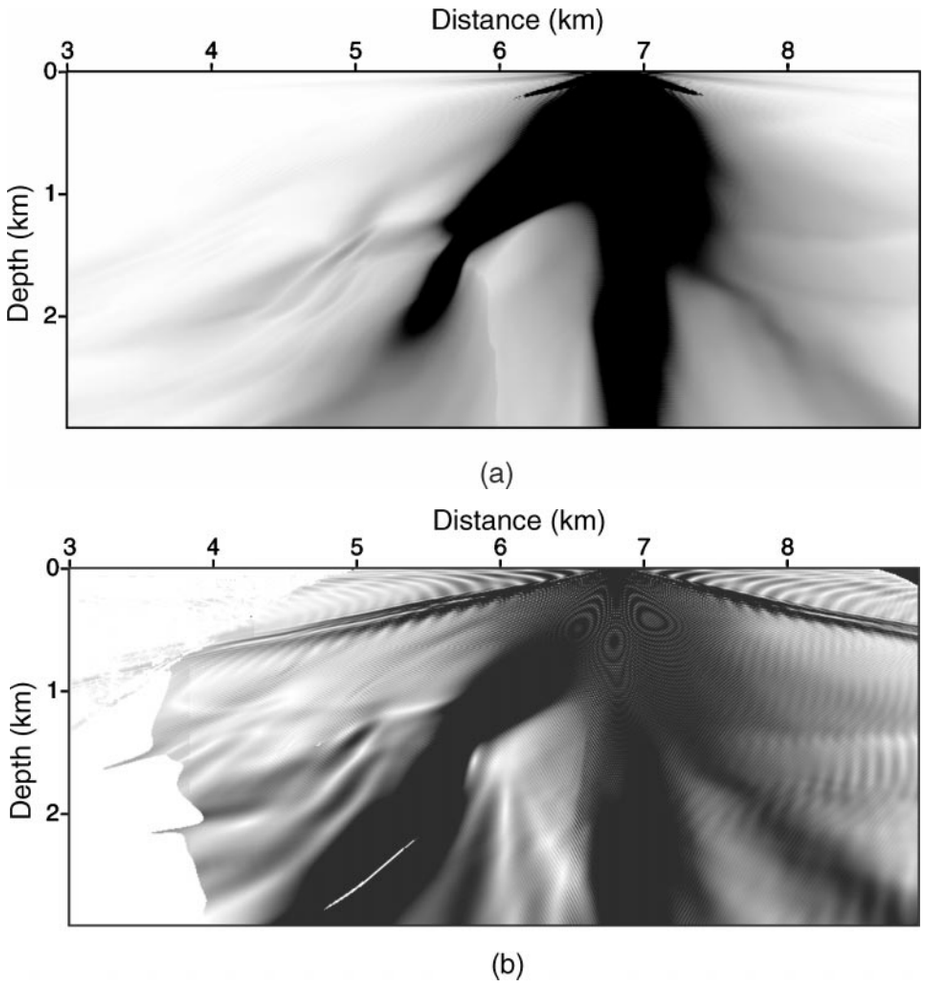


FIG. 4. (a) The absolute values of the most energetic amplitudes obtained from finite-difference solutions of the one-way wave equation, and (b) the absolute values of amplitudes computed by our algorithm for the 6%-smoothed Marmousi model.

migration that uses ray-based methods or eikonal equation solvers, the total cost of the 3D Kirchhoff migration mainly depends upon the aperture size, a massive input/output process, and a computation time of traveltimes corresponding to a given aperture volume. Furthermore, the computing time of 3D Kirchhoff migration is, in general, largely affected by the elaborate bookkeeping software used to read 3D traveltimes, hardware itself, and the storage amount of the hardware. When applying our new algorithms to the 3D Kirchhoff migration, we face almost the same complexities as we do when using the ray-based methods and eikonal traveltime computation algorithms. In our numerical example for 3D Kirchhoff migration for the 3D SEG/EAGE salt model, the traveltime computation roughly took 70% of the total computation time when the first method (taking logarithm of single-frequency displacements) is used and 80% when the second method (differentiating displacements with respect to $\omega$) is used.

We compared our second method of computing the approximately most energetic traveltimes by solving paraxial one-way wave equation at two frequencies with Nichols' (1996) method of calculating the most energetic traveltimes by solving the paraxial one-way wave equation at 8–16 frequencies. If we only consider how many frequencies are used for our second method and Nichols' (1996) method to compute the traveltimes, our second method reduces time consumed for calculating traveltime by at least 75% of that by Nichols' (1996) method. Of course, there is a slight reduction in terms of accuracy of traveltimes obtained by our second method. For the first-arrival traveltimes, our first algorithm is comparable to ray-based traveltime methods and eikonal equation solvers as long as we use optimized sparse matrix solvers such as a nested-dissection solver (George and Liu, 1981) or a multifrontal solver (Kim and Kim, 1999).

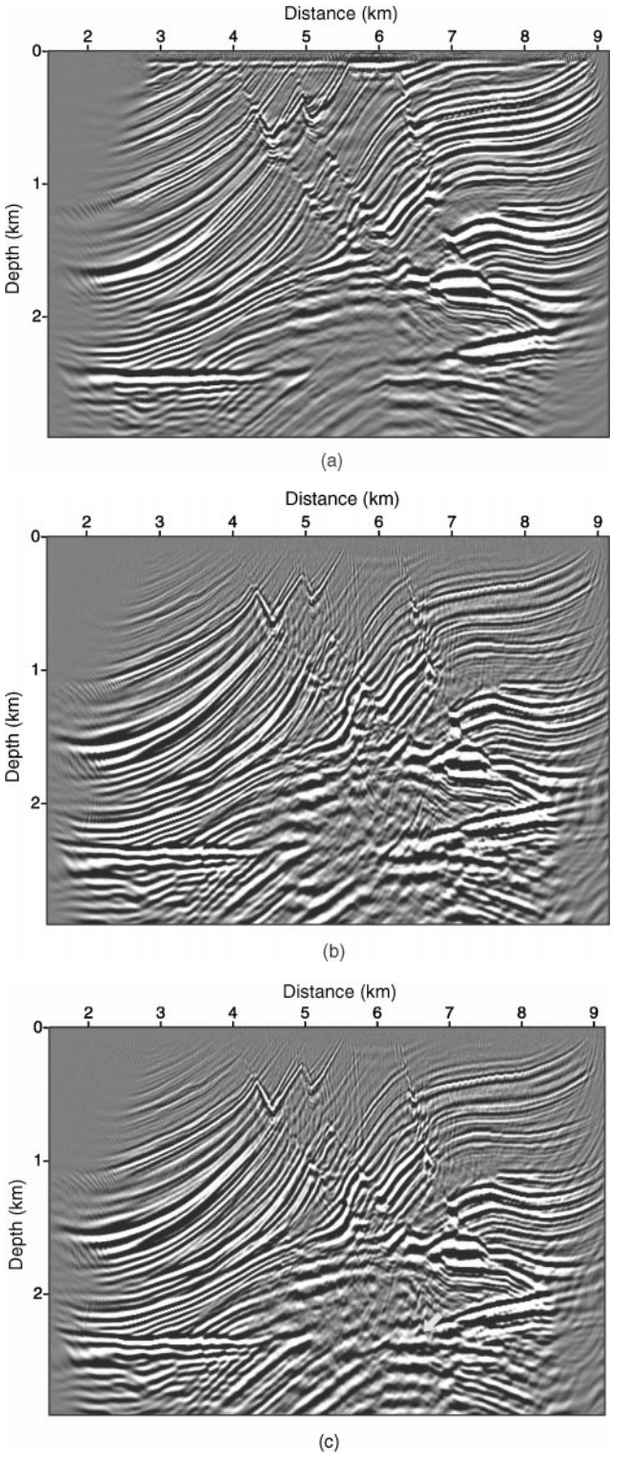


FIG. 5. Prestack Kirchhoff migration images produced by using (a) the most energetic traveltimes, and traveltimes obtained by (b) the first and (c) the second method for the 6%-smoothed Marmousi structure.

## CONCLUSIONS

By using the Fourier shifting theorem, we have developed two efficient methods of computing traveltimes necessary for imaging from any of the frequency-domain downward-continuation algorithms currently used in wave-equation migration. The first method is to extract traveltimes from the phase of the wavefield at a single complex angular frequency; the second method is to use the derivative of wavefield with respect to $\omega$ by approximating the derivative via the

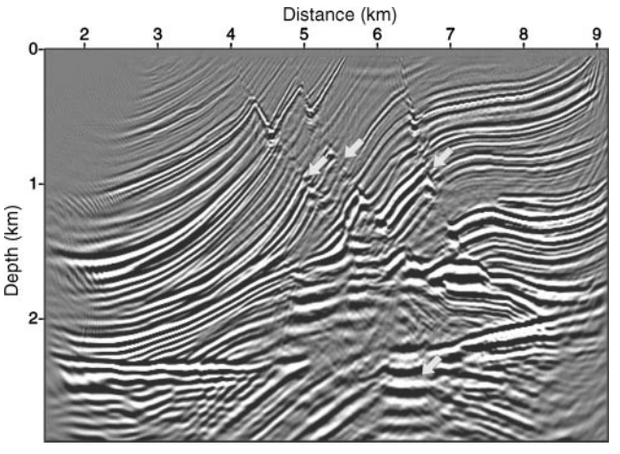


FIG. 6. Prestack Kirchhoff migration images produced with the approximately most energetic traveltimes and amplitudes computed by the second method for the 6%-smoothed Marmousi structure.

finite-difference method. By comparing the traveltimes obtained by our two methods with the most energetic traveltimes obtained from finite-difference solutions of the one-way wave equation, we see that the first method yields first-arrival traveltimes whereas the second method gives traveltimes that are closer to the most energetic traveltimes. The Kirchhoff migration images obtained by the first and second methods show that the second method gives better images. The second method also makes it possible to incorporate the amplitudes approximate to the seismic frequency band in Kirchhoff migration, which enhances the images.

However, the second traveltime calculation method has a problem yet to be solved: it is unstable for the case of the events following the first-arrival event having nearly the same amplitudes as that of the first-arrival event. Nevertheless, the second algorithm has a significant meaning that it provides the

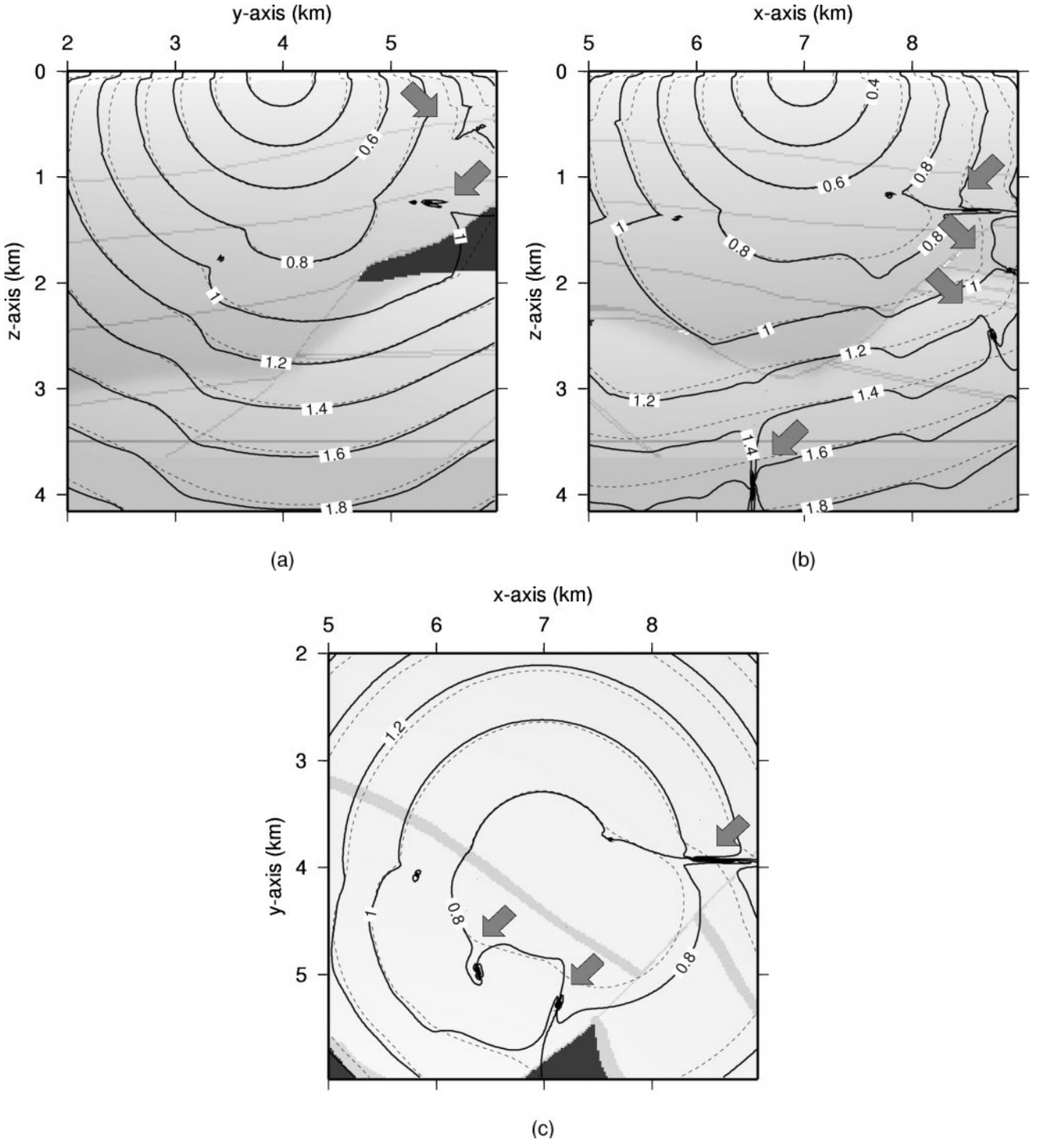


FIG. 7. Traveltime contours by the first (dotted line) and the second method (solid line) at (a) $x = 6.99$ km, (b) $y = 3.99$ km, and (c) $z = 1.4$ km for the 3D SEG/EAGE salt model.

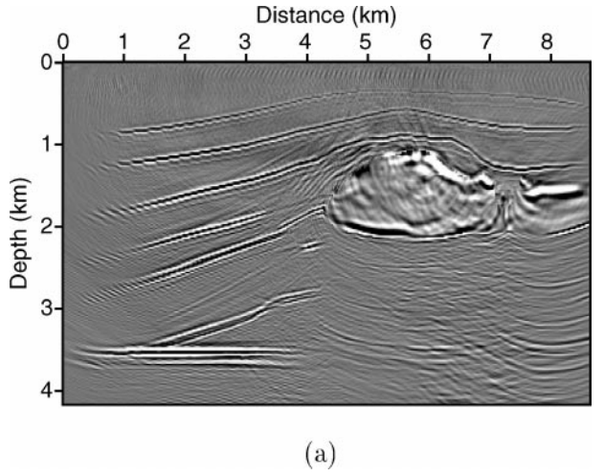


(a)

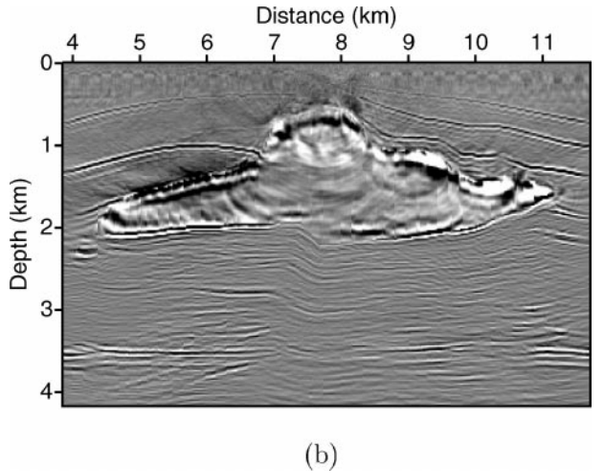


(b)

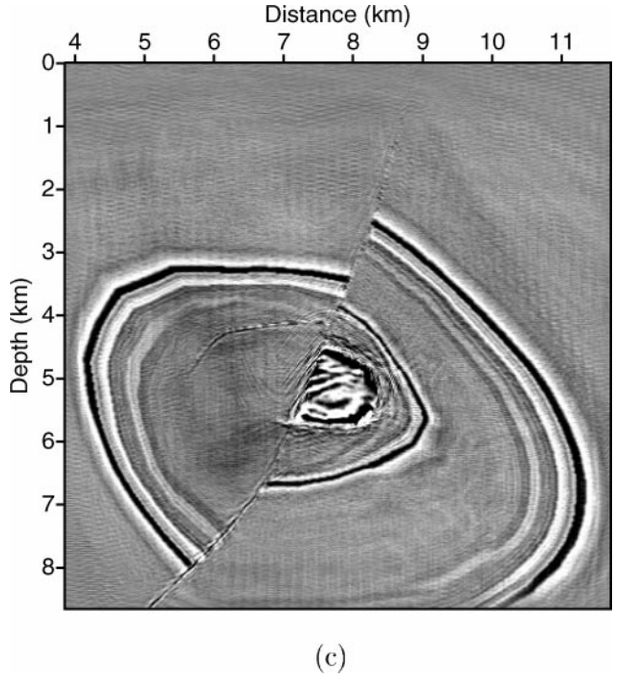


(c)

FIG. 8. Kirchhoff-migrated images using traveltimes produced with the first method at (a) $x = 8.84$ km, (b) $y = 5.74$ km, and (c) $z = 0.64$ km for the 3D SEG/EAGE salt model.

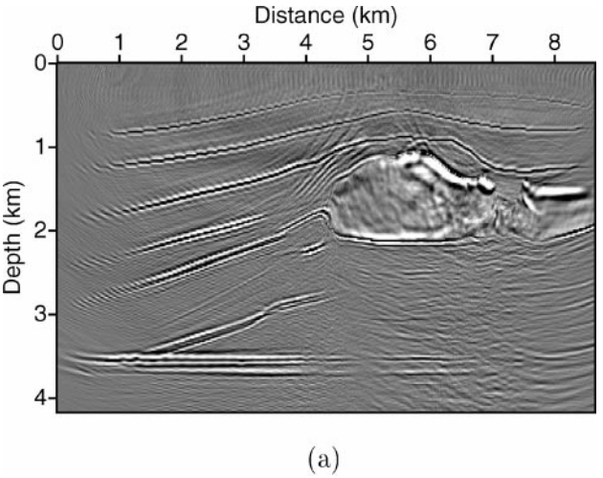


(a)

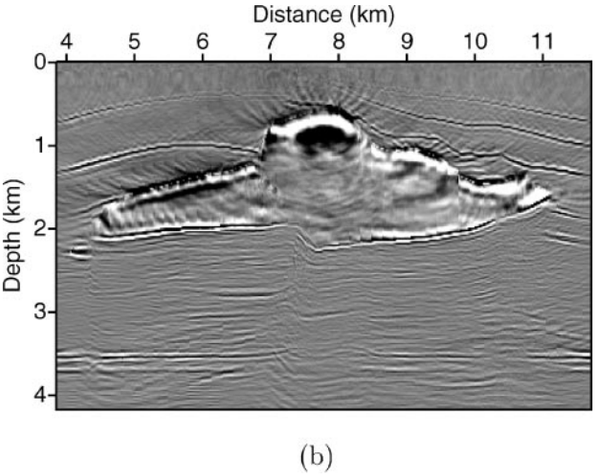


(b)

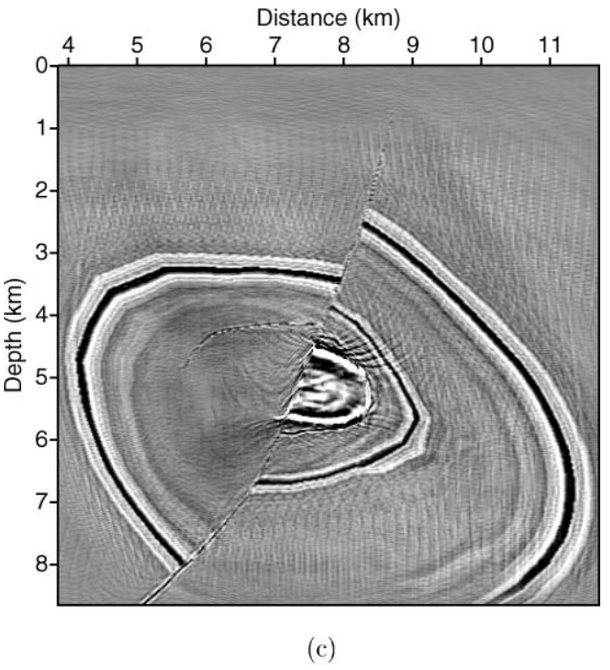


(c)

FIG. 9. Kirchhoff-migrated images using traveltimes produced with the second method at (a) $x = 8.84$ km, (b) $y = 5.74$ km, and (c) $z = 0.64$ km for the 3D SEG/EAGE salt model.

first step towards developing a method which generates temporally time-windowed seismograms including the most energetic events by frequency-domain wave-equation modeling.

## ACKNOWLEDGMENTS

This work was financially supported by National Laboratory Project of Ministry of Science and Technology, Brain Korea 21 project of the Korea Ministry of Education, and grant No. R03-2000-000-00003-0 from the Basic Research Program of the Korea Science & Engineering Foundation. We thank Korea Institute of Science and Technology Information for supporting computational resources of IBM Regatta power 4 for the computing 3D migration image.

## REFERENCES

Berkhout, A. J., 1979, Steep dip finite-difference migration: Geophys. Prosp., **27**, 196–213.
Cao, S., and Greenhalgh, S., 1994, Finite-difference solution of the eikonal equation using an efficient, first-arrival, wavefront tracking scheme: Geophysics, **59**, 632–643.
Cassell, B. R., 1982, A method for calculating synthetic seismogram in laterally varying media: Geophys. J. Roy. Astr. Soc., **38**, 9–19.
Claerbout, J. F., 1985, Imaging the earth's interior: Blackwell Scientific Publications.
Cerveny, V., Molotkpv, I. A., and Psencik, I., 1977, Ray methods in seismology: Univ. of Karlova Press.
Coultrip, L., 1993, High-accuracy wavefront tracing calculation: Geophysics, **58**, 284–292.
Geoltrain, S., and Brac, J., 1993, Can we image complex structures with first-arrival traveltime?: Geophysics, **58**, 564–575.
George, A., and Liu, J. W., 1981, Computer solution of large sparse positive definite systems: Prentice-Hall, Inc.
Kim, J. H., and Kim, S. J., 1999, A multifrontal solver combined with graph partitioners: Am. Inst. Aeronautics and Astronautics J., **38**, 964–970.
Lee, M. W., and Suh, S. Y., 1985, Optimization of one-way wave equation: Geophysics, **50**, 1634–1637.
Ma, Z., 1981, Finite-difference migration with higher-order approximation: Presented at the 1981 joint meeting of the China Geophys. Soc. and Soc. Expl. Geophys.
Nichols, D. E., 1996, Maximum energy traveltimes calculated in the seismic frequency band: Geophysics, **61**, 253–263.
Osman, O. M., and Robinson, E. A., Eds., 1996, Seismic source signature estimation and measurement: Soc. Expl. Geophys.
Podvin, P., and Lecomte, I., 1991, Finite-difference computation of traveltimes in very contrasted velocity models: A massively parallel approach and its associated tools: Geophys. J. Internat., **105**, 271–284.
Popovici, A. M., 1991a, Finite-difference traveltime maps: Stanford Expl. Project Rpt. **70**, 245–256.
——— 1991b, Stability of finite-difference traveltime algorithms: Stanford Expl. Project Rpt. **72**, 135–138.
Qin, F., Olsen, K. B., Luo, Y., and Schuster, G. T., 1990, Solution of the eikonal equation by a finite-difference method: 60th Ann. Internat. Mtg., Soc. Expl. Geophys., Expanded Abstracts, 1004–1007.
Schneider, W. A., Jr., 1995, Robust and efficient upwind finite-difference traveltime calculations in three dimensions: Geophysics, **60**, 1108–1117.
Sethian, J. A., and Popovici, A. M., 1999, 3-D traveltime computation using the fast marching method: Geophysics, **64**, 516–523.
Shin, C., Min, D.-J., Marfurt, K. J., Lim, H. Y., Yang, D., Cha, Y., Ko, S., Ha, T., and Hong, S., 2002, Traveltime and amplitude calculations using the damped wave solution: Geophysics, **67**, 1637–1647.
Sun, Y., 1992, Computation of 2-D multiple arrival travel time fields by an interpolative shooting method: 62nd Ann. Internat. Mtg, Soc. Expl. Geophys., Expanded Abstracts, 1320–1323.
Um, J., and Thurber, C., 1987, A fast algorithm for two-point seismic ray tracing: Bull. Seism. Soc. Am., **77**, 972–986.
Van Trier, J., and Symes, W. W., 1991, Upwind finite-difference calculation of traveltimes: Geophysics, **56**, 812–821.
Vidale, J. E., 1988, Finite-difference travel time calculation: Bull. Seism. Soc. Am., **78**, 2062–2076.
Vinje, V., Astebol, K., Lversen, E., and Gjoystdal, H., 1999, 3-D ray modeling by wave front construction in open models: Geophysics, **64**, 1912–1919.
Zhu, J., and Lines, L. R., 1998, Comparison of Kirchhoff and reverse-time migration methods with applications to prestack depth imaging of complex structures: Geophysics, **63**, 1166–1176.

## APPENDIX A

### THE SHIFTING THEOREM OF FOURIER TRANSFORMS

Frequency-domain solutions $\tilde{u}(\omega)$ are obtained from time-domain solutions by

$$\tilde{u}(\omega) = \int_{-\infty}^{\infty} u(t) e^{-i\omega t} dt. \tag{A-1}$$

If we shift the angular frequency by $\omega_o$, we obtain

$$\begin{aligned} \tilde{u}(\omega + \omega_o) &= \int_{-\infty}^{\infty} u(t) e^{-i(\omega+\omega_o)t} dt \\ &= \int_{-\infty}^{\infty} u(t) e^{-i\omega t} e^{-i\omega_o t} dt. \end{aligned} \tag{A-2}$$

In this case, time-domain solutions are written as

$$u(t) = \int_{-\infty}^{\infty} \tilde{u}(\omega + \omega_o) e^{i\omega t} e^{i\omega_o t} d\omega. \tag{A-3}$$

From these equations, we know that shifting in the frequency is expressed by exponential.

When we use complex angular frequency $\omega_\epsilon = \omega + i\epsilon$, the shifting is the imaginary part. In this case, the shifting can be described by decaying exponentials:

$$\begin{aligned} u(t) &= \int_{-\infty}^{\infty} \tilde{u}(\omega_\epsilon) e^{i\omega_\epsilon t} d\omega \, , \\ &= \int_{-\infty}^{\infty} \tilde{u}(\omega_\epsilon) e^{i\omega t} e^{-\epsilon t} d\omega. \end{aligned} \tag{A-4}$$